JACS
JOURNAL OF THE AMERICAN CHEMICAL SOCIETY

Article

pubs.acs.org/JACS

# Mechanism of Self-Assembly Process and Seeded Supramolecular Polymerization of Perylene Bisimide Organogelator

Soichiro Ogi,[†] Vladimir Stepanenko,[†] Kazunori Sugiyasu,[‡] Masayuki Takeuchi,[‡] and Frank Würthner*[,†]

[†]Institut für Organische Chemie and Center for Nanosystems Chemistry, Universität Würzburg, Am Hubland, 97074 Würzburg, Germany

[‡]Organic Materials Group, Polymer Materials Unit, National Institute for Materials Science (NIMS), 1-2-1 Sengen, Tsukuba 305-0047 Ibaraki, Japan

Supporting Information

**ABSTRACT:** The mechanism of supramolecular polymerization has been elucidated for an archetype organogelator molecule composed of a perylene bisimide aromatic scaffold and two amide substituents. This molecule self-assembles into elongated one-dimensional nanofibers through a cooperative nucleation−growth process. Thermodynamic and kinetic analyses have been applied to discover conditions (temperature, solvent, concentration) where the spontaneous nucleation can be retarded by trapping of the monomers in an inactive conformation, leading to lag times up to more than 1 h. The unique kinetics in the nucleation process was confirmed as a thermal hysteresis in a cycle of assembly and disassembly processes. Under appropriate conditions within the hysteresis loop, addition of preassembled nanofiber seeds leads to seeded polymerization from the termini of the seeds in a living supramolecular polymerization process. These results demonstrate that seeded polymerizations are not limited to special situations where off-pathway aggregates sequester the monomeric reactant species but may be applicable to a large number of known and to be developed molecules from the large family of molecules that self-assemble into one-dimensional nanofibrous structures. Generalizing from the mechanistic insight into our seeded polymerization, we assert that a cooperative nucleation−growth supramolecular polymerization accompanied by thermal hysteresis can be controlled in a living manner.

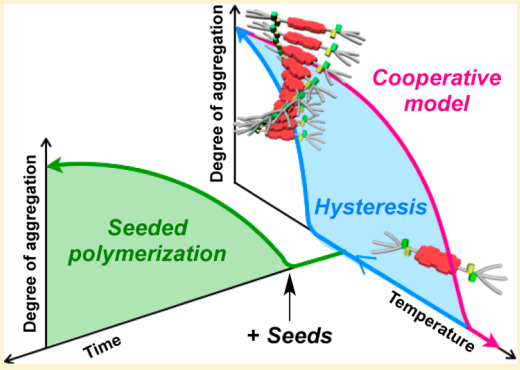


## INTRODUCTION

Supramolecular polymers and organogels based on π-conjugated molecules constitute an important class of materials for various applications including the areas of organic electronics and photonics.[1] However, there are only few examples where functional properties such as charge or exciton mobility were tailored by supramolecular design, whereas most of the commonly applied π-conjugated materials in organic electronics were developed only from molecule properties consideration.[2] Although the function of such organic materials originates from the highly ordered assemblies, and thus sensitively dependent on the molecular organization, it is still elusive to program the molecular self-assembly pathway over several levels of hierarchy from dilute monomer solution up to a bulk material. In particular recent research has shown that already the first steps of the self-assembly pathway may lead toward kinetically trapped self-assembly products that determine the final outcome in terms of nanostructure and function.[3] These findings highlight the necessity to deepen our knowledge about self-assembly mechanisms to control supramolecular polymerization with similar sophistication as accessible in covalent polymerization. In this regard, seeded polymerization, as observed in actin and flagellin polymerization,[4] is a promising approach to obtain well-defined nanostructures.[5] For instance, Manners, Winnik, and co-workers reported that seeded polymerization of amphiphilic block copolymers yielded micelles with controlled length through an epitaxial crystallization process.[6] Moreover, this methodology was extended to producing block micelles that further assembled into hierarchical architectures.[7] Similarly, Aida and co-workers achieved a p−n heterojunction through seeded growth of hexabenzocoronene derivatives into semiconducting nanotubes.[8] Most recently, the "seeding" approach has been applied for the first time by Sugiyasu, Takeuchi, and co-workers to control the structure of supramolecular polymers with a unimolecular width.[9] They have demonstrated living supramolecular polymerization of porphyrin-based monomers, leading to supramolecular polymers with controlled length and narrow polydispersity. However, to the best of our knowledge, no further examples are known so far that demonstrate seeded supramolecular polymerization.[10]

Perylene bisimides (PBIs) have evolved as one of the most intensively investigated classes of π-conjugated molecules during the last two decades.[11] Besides their outstanding optical and electronic properties that enable applications in organic

Received: November 25, 2014
Published: February 17, 2015

ACS Publications © 2015 American Chemical Society



DOI: 10.1021/ja511952c
J. Am. Chem. Soc. 2015, 137, 3300−3307

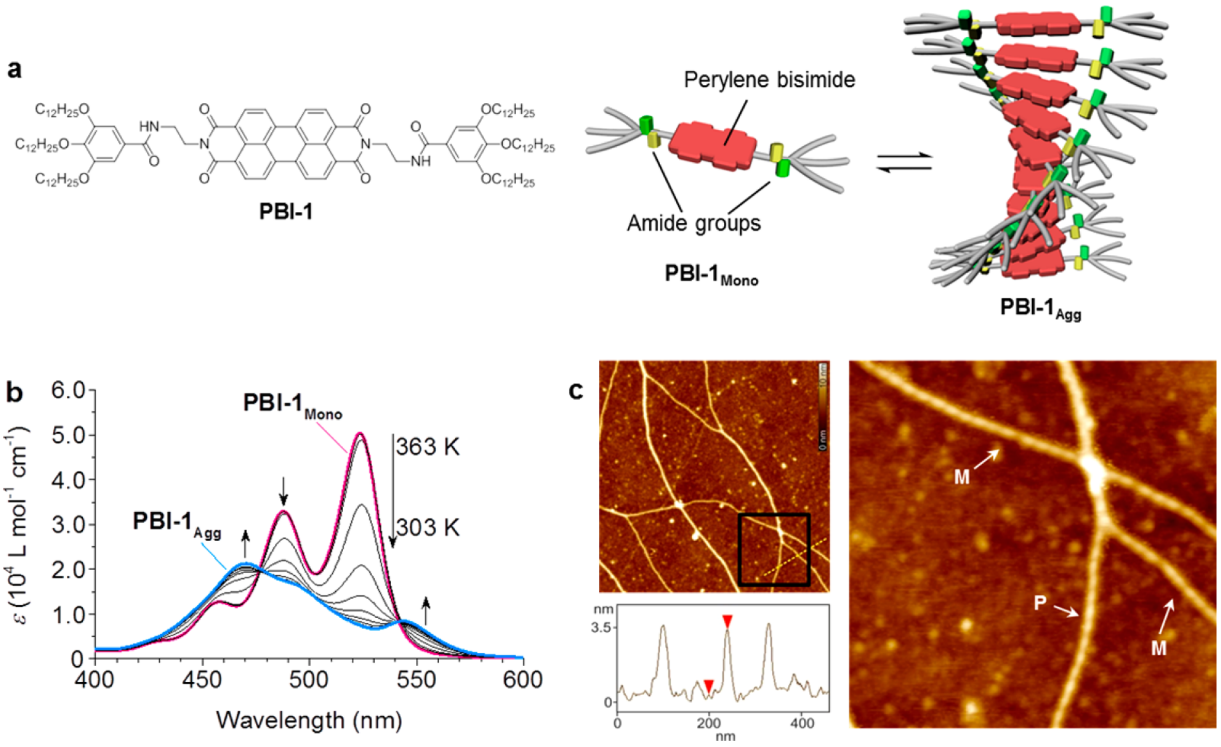


**Figure 1.** (a) Chemical structure of **PBI-1** used for the studies on the seeded polymerization, and schematic representation of the hydrogen-bond-directed self-assembly behavior of **PBI-1**. (b) Temperature-dependent absorption spectral changes of **PBI-1** in MCH/toluene (2:1, v/v) observed during cooling process from 363 K (pink line) to 303 K (blue line). Condition: $c_T = 1.0 \times 10^{-5}$ M. (c) Left top, AFM height image (1.5 × 1.5 $\mu$m, the $z$ scale is 10 nm) of **PBI-1**$_{Agg}$, spin-coated (3000 rpm) onto silicon wafers from the MCH/toluene solutions. Left bottom, cross-section analysis corresponding to the yellow dashed line. Right, height image (0.46 × 0.46 $\mu$m, the $z$ scale is 10 nm) of the region enclosed with the black line.

electronics, photovoltaics, and photonics,[12] these molecules exhibit most suitable molecular recognition units for $\pi-\pi$ stacking and hydrogen bonding as desired to tailor supramolecular packing and self-assembly processes.[13] Almost a decade ago, we designed an organogelator based on a PBI derivative bearing amide groups and solubilizing alkyl chains at the imide positions (**PBI-1** in Figure 1). As shown in several previous studies, this molecule self-assembles by the concerted hydrogen-bonding and $\pi-\pi$ stacking interactions into highly defined one-dimensional helical aggregates that gelate a broad range of organic solvents.[14] Due to the similarity of the molecular structure with that of the recently reported first example for living supramolecular polymerization by seeding approach,[9] we decided to re-explore the self-assembly of **PBI-1** to address the query whether the seeding approach can be extended to this building block.

An essential requirement to accomplish a living supramolecular polymerization is a deep understanding of the supramolecular polymerization mechanism on the basis of both thermodynamic and kinetic insights.[5,9,10] Based on the mechanistic understanding of the seeding approach,[5] we postulate that seeded polymerization is effective under the following conditions: (1) Polymerization undergoes through a cooperative (nucleation–elongation) model,[15] so that the growth of the fiber by newly added monomers propagates only from the seeds; (2) spontaneous nucleation is retarded and thus supramolecular polymerization is controlled kinetically; and (3) seeds can be prepared separately to initiate the supramolecular polymerization externally. To clarify the generality of this concept, we have investigated in detail the supramolecular polymerization of **PBI-1** from mechanistic viewpoints. Our present results reveal that monomeric **PBI-1** self-assembles into supramolecular polymers through nucleation followed by elongation processes. Importantly, the monomeric state of **PBI-1** is kinetically trapped and inactivated in low-polarity solvents, so that the spontaneous nucleation is temporarily retarded. Based on the unique kinetics of the nucleated polymerization, we have succeeded in demonstrating seeded polymerization of **PBI-1**.

## RESULTS AND DISCUSSION

**Temperature-Dependent Supramolecular Polymerization.** The self-assembly behavior of **PBI-1** has been investigated by temperature-dependent UV–vis spectroscopy, which is a convenient method to identify the supramolecular polymerization mechanism and to distinguish growth processes according to the isodesmic (equal-K) or the cooperative (nucleation–elongation) model.[16] Figure 1b shows the temperature-dependent absorption spectra of **PBI-1** in a solvent mixture of methylcyclohexane (MCH) and toluene with a volume ratio of MCH/toluene = 2:1 at a total **PBI-1** concentration ($c_T$) of $1.0 \times 10^{-5}$ M. Upon cooling the solution from 363 to 303 K (at a rate of 1 K min$^{-1}$), the absorption maximum is blue-shifted with a decrease in absorbance. These spectral features are characteristic for the transition from monomeric (**PBI-1**$_{Mono}$) to a aggregate state (**PBI-1**$_{Agg}$).[14] Atomic force microscopy (AFM) images showed that **PBI-1**$_{Agg}$ is a supramolecular polymer with a unimolecular width of 3.2 ± 0.1 nm and equal amounts of both left- and right-handed helices in accordance with our previous work (Figure 1c).[14c] Although the width and observed helicity are fully consistent with the model of a single supramolecular fiber (Figure 1a), we


DOI: 10.1021/ja511952c
J. Am. Chem. Soc. 2015, 137, 3300–3307

like to emphasize the propensity of these fibers for bundling, which is nicely revealed in the closer AFM image section in Figure 1c where individual fibers of opposing helicity merge.

The temperature-dependent degree of aggregation ($\alpha_{Agg}$) estimated from the apparent absorption coefficients at $\lambda$ = 523 nm observed in the cooling process revealed that the supramolecular polymerization proceeded abruptly at the critical temperature of 342 K (Figure 2a, blue dots). The

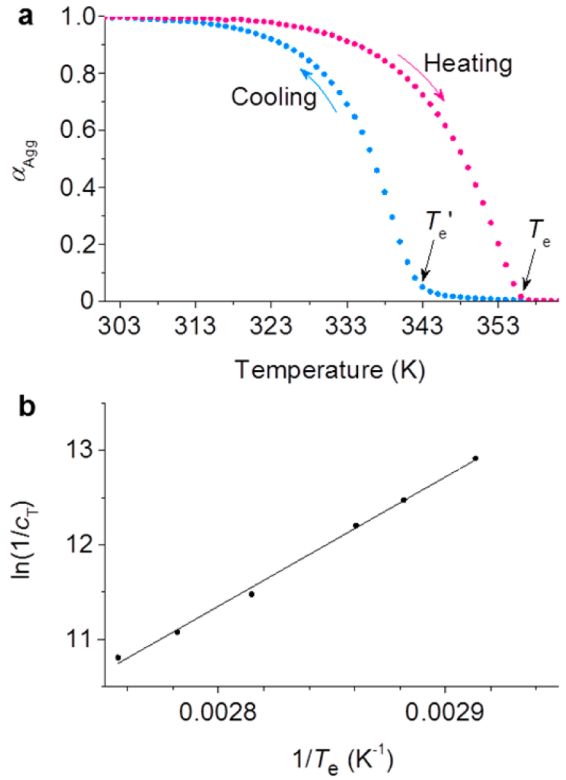


**Figure 2.** (a) Temperature-dependent degree of **PBI-1**$_{Agg}$ ($\alpha_{Agg}$) calculated from the apparent absorption coefficients at $\lambda$ = 523 nm observed in the cooling (blue) and heating (pink) processes at a rate of 1 K min$^{-1}$. Condition: $c_T$ = 1.0 × 10$^{-5}$ M, MCH/toluene (2:1, v/v). (b) Natural logarithm of the reciprocal $c_T$ as a function of the reciprocal $T_e$ showing the linear relationship (correlation coefficient 0.998).[17]

observed nonsigmoidal transition implies a cooperative aggregation process of **PBI-1**$_{Mono}$.[15,16] Interestingly, a thermal hysteresis was observed in the disassembly process from the fibrous **PBI-1**$_{Agg}$ to **PBI-1**$_{Mono}$ upon heating at a rate of 1 K min$^{-1}$ (Figure 2a, pink dots), indicating that the critical temperatures in the cooling and heating processes are clearly distinguished as $T_e'$ (342 K) and $T_e$ (355 K), respectively. Moreover, the value of $T_e'$ was shifted to a higher temperature as the cooling rate was decreased successively from 1 to 0.1 K min$^{-1}$ (Supporting Information Figure S1, blue). These results clearly indicate that the supramolecular polymerization of **PBI-1**$_{Mono}$ is not able to follow the rapid temperature change and is accordingly under kinetic control. In contrast, no notable effect of heating rate on the $T_e$ was observed, indicating the disassembly process occurs under thermodynamic control (Supporting Information Figure S1, pink). The nonsigmoidal transition could be properly fitted by using the cooperative model proposed by Meijer, Schenning and co-workers,[15a,17] giving the elongation enthalpies of $\Delta H_e$ = −108.1 kJ mol$^{-1}$ and $T_e$ = 355.3 K at the given concentration of 1.0 × 10$^{-5}$ M (Supporting Information Figure S2 and Table S1). Upon diluting the total concentration of **PBI-1** ($c_T$), the $T_e$ decreased with a linear relationship in the van't Hoff plot, from which the standard enthalpy ($\Delta H°$) and entropy ($\Delta S°$) were estimated to be −114 kJ mol$^{-1}$ and −224 J mol$^{-1}$ K$^{-1}$, respectively (Figure 2b). The $\Delta H°$ value is very close to that of $\Delta H_e$ (−108.1 kJ mol$^{-1}$) determined by the cooperative model and comparable to the earlier reported value for the structurally similar porphyrin derivative.[9] Furthermore, the Goldstein−Stryer model is applicable to the concentration-dependent data at 343 K (Supporting Information Figure S3 and Table S2),[18] affording an elongation equilibrium constant of $K_E$ = 4.1 × 10$^5$ M$^{-1}$, which is in agreement with the value of $K_E$ (4.6 × 10$^5$ M$^{-1}$) calculated from $\Delta H°$ and $\Delta S°$ values. All these analytical results provide clear evidence that the fibrous **PBI-1**$_{Agg}$ was formed through a cooperative nucleation−growth process.

**Kinetic Trapping.** Regarding the data observed in the cooling process, it should be noted that the van't Hoff plot showed again a linear relationship but yielded a standard enthalpy ($\Delta H°'$) value of −67 kJ mol$^{-1}$, which is vastly different from the $\Delta H°$ value (−114 kJ mol$^{-1}$) determined from the data obtained in the heating process (Supporting Information Figure S4). Additionally, it was not possible to determine thermodynamic parameters by fitting the concentration-dependent data to the Goldstein−Stryer model (Supporting Information Figure S5). These failures are apparently caused by the kinetic effect on the supramolecular polymerization process.

Supramolecular polymerization is strongly influenced by the solvation properties of the utilized solvent.[19] We have previously reported that aggregate nanofibers of **PBI-1** are also formed in pure toluene.[14a] Thus, we explored the solvent effect on the nucleation kinetics of **PBI-1**. The polymerization and disassembly processes were monitored as a function of temperature at a rate of 1 K min$^{-1}$, in which a thermal hysteresis of nonsigmoidal transitions was observed as well with values of $T_e'$ = 292 K and $T_e$ = 317 K at a given concentration of 2 × 10$^{-5}$ M (Supporting Information Figure S6, filled circles). These temperatures are lower than those determined in MCH/toluene solution, reflecting the fact that the supramolecular polymer of **PBI-1** is thermodynamically less stable in pure toluene than in MCH/toluene solution. This solvent effect is attributed to the better solvation of the aromatic $\pi$-surface of PBIs by toluene, which is a more polarizable solvent with higher refractive index.[19] In accordance the van't Hoff plot based on the $T_e$ value (i.e., thermodynamic control) in pure toluene yielded $\Delta H°$ and $\Delta S°$ values of −90 kJ mol$^{-1}$ and −195 J mol$^{-1}$K$^{-1}$, respectively (Supporting Information Figure S7). We note that these thermodynamic parameters of the nucleation−growth process are influential on the kinetic behavior of the self-assembly of **PBI-1** as the system is based on the interplay of the coupled equilibria (see below).

In previously reported systems, kinetic control over a nucleated supramolecular polymerization has been only achieved through a complex interplay of two aggregation pathways.[9,20] Namely, monomeric species were trapped kinetically as a metastable aggregate, which is an off-pathway intermediate with regard to the thermodynamically stable products; thus, the spontaneous nucleation was inhibited. In contrast to the pathway complexity in these systems,[9,20] the **PBI-1**$_{Mono}$ prevails in a kinetically trapped unimolecular state and no off-pathway aggregate of **PBI-1** was observed. This


DOI: 10.1021/ja511952c
J. Am. Chem. Soc. 2015, 137, 3300−3307

peculiar type of kinetic trapping can be rationalized by the formation of intramolecular hydrogen bonds between the amide hydrogens of the benzamide units and the imide carbonyl oxygens of the PBI (Scheme 1). Computer-generated

**Scheme 1. Chemical Equilibrium between a Reactive Open and a Trapped Closed Conformation of PBI-$1_{Mono}$, Where the Dodecyl Groups Are Simplified As R**

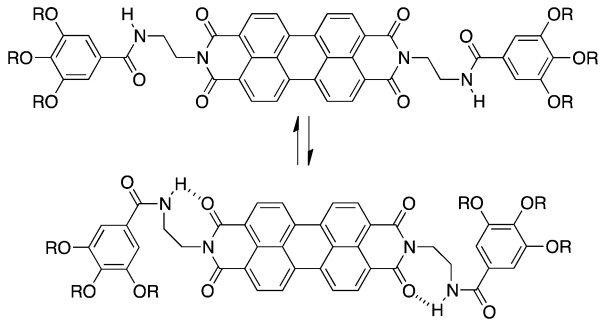

molecular models indeed imply that the intramolecular hydrogen bond formation retains the trialkoxy benzamide groups into spatial positions that shield the PBI $\pi$-surfaces and concomitantly prevent the self-assembly of the **PBI-1** molecules (Scheme 1, Supporting Information Figure S8).

In low-polarity solvents that lack hydrogen-bond donor and acceptor capabilities, such intramolecular hydrogen bonds are well established for up to nine-membered rings since the pioneering work of Gellman et al. and Nowick et al. on conformation-directing effects of bis-amides and bis-ureas.[21,22] Following these authors work we could indeed obtain sound evidence for the presence of hydrogen bonds in deuterated toluene within the whole temperature range (Supporting Information Figure S9). Accordingly, only a very modest temperature-dependence of the chemical shift ($\Delta\delta/\Delta T$) of the amide proton at ~6.5 ppm is observed upon cooling from 369 to 323 K. This demonstrates the prevalence of a hydrogen-bonded amide group that experiences a similar shielding effect by the intramolecular hydrogen-bonding to the imide carbonyl at higher temperature and by the intermolecular hydrogen bonding to an amide carbonyl group at lower temperature. The reorganization from intra- to intermolecular hydrogen-bonded **PBI-1** is supported well by temperature-dependent absorption spectral changes corresponding to the transition from **PBI-$1_{Mono}$** to **PBI-$1_{Agg}$** in deuterated toluene (Supporting Information Figure S10). In contrast in more polar deuterated 1,1,2,2-tetrachloroethane, a pronounced temperature dependence of the chemical shift ($\Delta\delta/\Delta T$) of the amide proton is observed in the same temperature range that originates from a shift of the equilibrium from the stretched non hydrogen-bonded state at higher temperature to the hydrogen-bonded folded state at lower temperature (Supporting Information Figure S11). This result is well-explained by the fact that the hydrogen-bonded state is enthalpically more favorable, while the non-hydrogen-bonded state is entropically more favorable.[21] The shift of the equilibrium from non-hydrogen-bonded to intramolecular hydrogen-bonded conformations at lower temperatures could be further confirmed by Fourier-transform infrared (FT-IR) spectral measurement that revealed the appearance of a new stretching frequency at 3409 $cm^{-1}$ assigned to hydrogen-bonded amide hydrogens concomitant with a decrease in the intensity of the common band for non-hydrogen-bonded amide hydrogens at 3446 $cm^{-1}$ (Supporting Information Figure S12).[9] Notably, no $\pi-\pi$ stacking interaction between the perylene cores is evident for the given conditions in the UV–vis absorption bands which show the well-resolved vibronic structure of monomeric PBIs (Supporting Information Figure S13). These results corroborate that the amide hydrogens are hydrogen-bonded intramolecularly.

An interesting aspect of the hysteresis loop is that the monomeric state (**PBI-$1_{Mono}$**) is kinetically trapped and inactivated within the temperature range between $T_e$ and $T_e'$. For instance, at a concentration of $2 \times 10^{-5}$ M the critical temperatures $T_e'$ and $T_e$ were observed at 352 and 363 K, respectively, in MCH/toluene solution (2:1, v/v) (Supporting Information Figure S6, open square dots). The difference between the critical temperatures ($\Delta T_e = T_e - T_e'$) provides an effective range for inactivating **PBI-$1_{Mono}$** kinetically, which is determined by the energetic relationship between the inactive trapped hydrogen-bonded state and the non hydrogen-bonded state that is "active" for supramolecular polymerization. As shown in Figure 3, the effective range is shifted to a lower

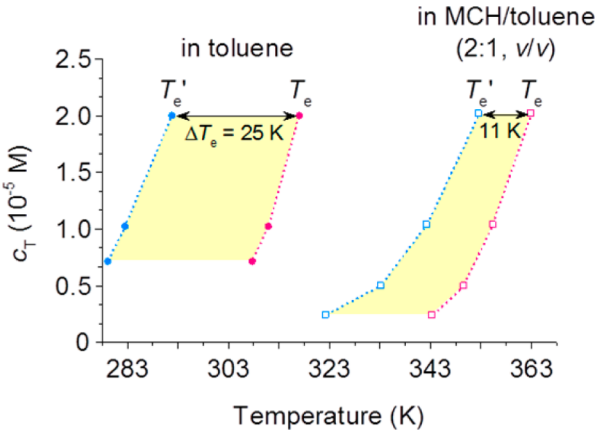


**Figure 3.** Values of $T_e'$ (blue) and $T_e$ (pink) observed in cooling and heating processes at a rate of 1 K $min^{-1}$, respectively, at different $c_T$ in MCH/toluene (2:1, v/v, □) and pure toluene (●). The yellow area shows the estimated effective range for stabilizing **PBI-$1_{Mono}$** kinetically.

temperature and becomes wider with decreasing the $c_T$. In other words, under the conditions in which the kinetic trap (i.e., intramolecular association process) is preferred over the supramolecular polymerization (i.e., intermolecular process), $\Delta T_e$ window can be expanded. Similarly, as the volume ratio of toluene increased from 33% to 100% (i.e., destabilizing the supramolecular polymer), both $T_e'$ and $T_e$ decreased by 60 and 46 K, respectively; accordingly, the $\Delta T_e$ increased from 11 to 25 K (Figure 3).

**Time-Dependent Supramolecular Polymerization.** The kinetically trapped state discussed above should eventually transform into the thermodynamically equilibrated supramolecular polymer over time. To gain insight into this time-dependent evolution, we monitored the absorption spectral changes as a function of time. The sample was prepared by fast cooling of (1) a MCH/toluene solution (2:1, v/v) and (2) a pure toluene solution of **PBI-1** ($c_T = 2 \times 10^{-5}$ M) from 368 to 298 K at a rate of ca. 25 K $min^{-1}$. Then, the measurement was started 2 min after the temperature was reached at 298 ± 0.1 K, and the spectra were taken in 1 min interval. The measurements for the MCH/toluene solution showed that the self-


DOI: 10.1021/ja511952c
J. Am. Chem. Soc. 2015, 137, 3300–3307

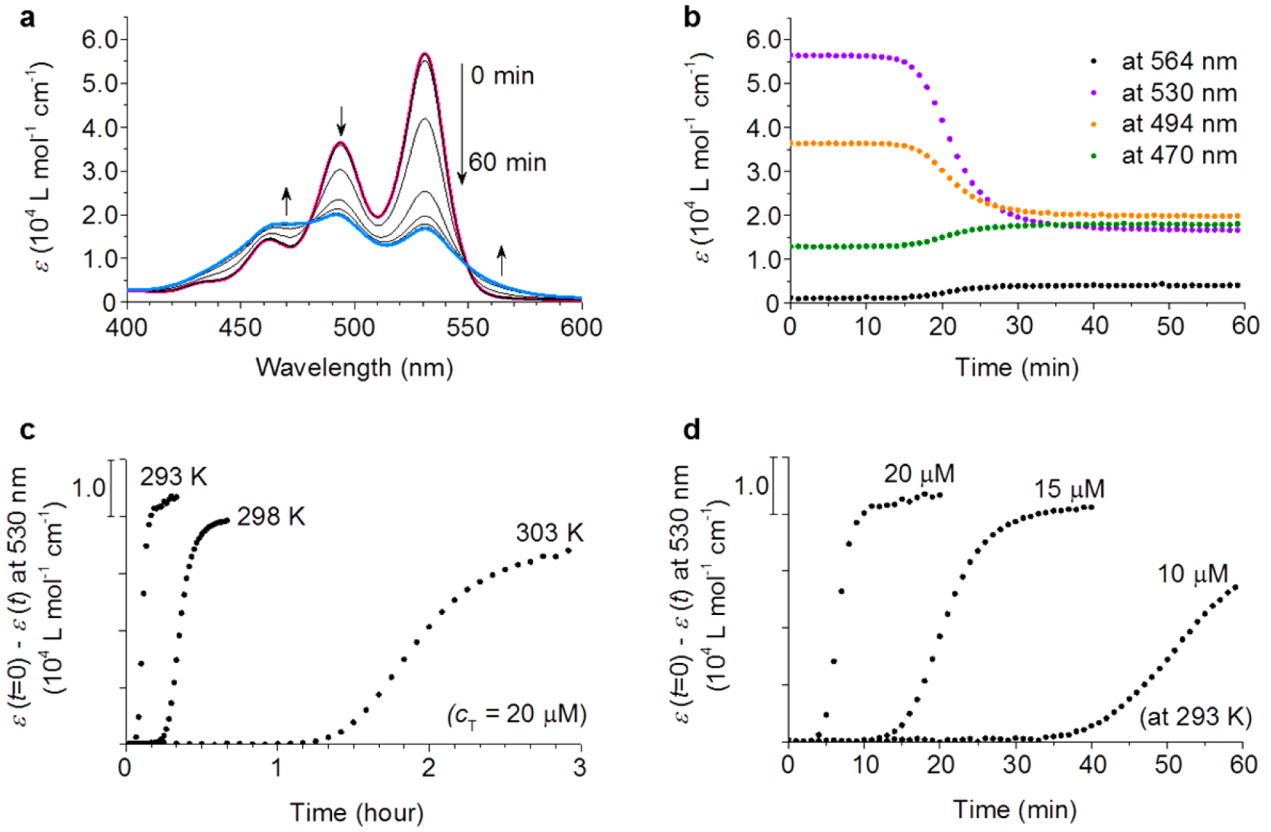


**Figure 4.** (a) Time-dependent absorption spectral changes of **PBI-1** in toluene observed after fast cooling from 368 to 298 K. Conditions: $c_T = 2 \times 10^{-5}$ M, 298 K. (b) Plots of $\varepsilon$ values at the given wavelength as a function of time observed in (a). (c,d) Time course of the aggregate formation in toluene at different temperatures at $2 \times 10^{-5}$ M (c) and at different concentrations at 293 K (d).

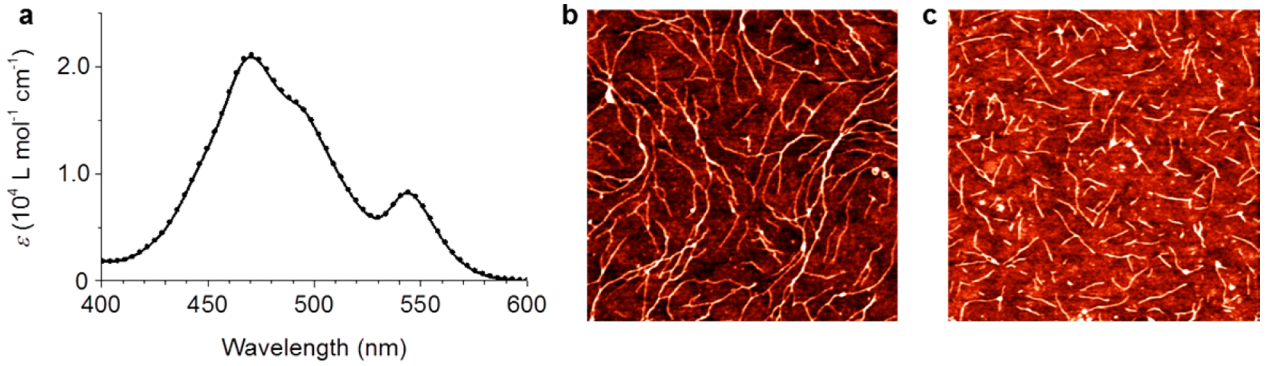


**Figure 5.** (a) Absorption spectra of **PBI-1**$_{Agg}$ (black dots) and **PBI-1**$_{Seed}$ (black line) in MCH/toluene (2:1, v/v) obtained by fast cooling without and with ultrasonic treatment, respectively. Conditions: $c_T = 1 \times 10^{-5}$ M, 293 K. (b,c) AFM height images (5 × 5 $\mu$m, the $z$ scale is 3 nm) of the **PBI-1**$_{Agg}$ (b) and **PBI-1**$_{Seed}$ (c), spin-coated (3000 rpm) onto silicon substrates from each solution.

assembly into aggregates was already almost completed after this short period of time (Supporting Information Figure S14) because the measurement temperature of 298 K is significantly lower than the $T_e'$ value of 352 K for the MCH/toluene solution (Figure 3, blue open squares). As such, the supramolecular polymerization easily prevails over the kinetic trap in MCH/toluene solution.

In contrast, for the toluene solution the measurement temperature is between $T_e$ and $T_e'$ (Figure 3, filled circles). Therefore, as expected the supramolecular polymerization proceeded with a different kinetic profile from the one observed in MCH/toluene mixture. Namely, the fast cooled toluene solution of **PBI-1** showed the absorption spectrum of the monomeric state, which transformed to aggregate with accompanying a significant lag time (Figure 4a,b). The sigmoidal transition is characteristic of an autocatalytic process that consists of nucleation and elongation processes.[9,23] The spontaneous nucleation is kinetically retarded, and this out-of-equilibrium monomeric state is trapped longer with increasing temperature (Figure 4c). Importantly, the lag time is also dependent on the total concentration of **PBI-1** ($c_T$): that is, the lower the $c_T$ is, the longer the lag time becomes (Figure 4d). This concentration dependence is opposite to the previously reported porphyrin based system in which the monomers were trapped as off-pathway aggregate.[9] Note that the lag time is extended with increasing fraction of the kinetically trapped


DOI: 10.1021/ja511952c
J. Am. Chem. Soc. 2015, 137, 3300−3307

monomers.[24] Accordingly, this result indicates that the kinetic trap in the present system is preferentially created under diluted conditions, which is consistent with our hypothesis based on the *intramolecular* hydrogen-bond formation (Scheme 1). Given the unique time-dependent evolution, the lag time can be set to even 1 h at an initial concentration of $2 \times 10^{-5}$ M and a temperature of 303 K in toluene, which is long enough to perform the following seeded polymerization experiments.

**Seeded Supramolecular Polymerization.** The slow kinetics, which accompanies the lag time to reach the thermodynamic equilibrium, allowed us to investigate whether the supramolecular polymerization can be initiated through a "seeding" approach. The seed of **PBI-1** aggregate (**PBI-1**$_{Seed}$) was prepared by applying sonication to a hot **PBI-1** solution in MCH/toluene (2:1, v/v) for 5 min in a water bath at 293 K. The absorption spectrum of **PBI-1**$_{Seed}$ was consistent with that of **PBI-1**$_{Agg}$ obtained without additional ultrasonic treatment (Figure 5a). AFM images showed that **PBI-1**$_{Seed}$ consists of nanofibers with a number-average length ($L_n$) of 290 nm, which are much shorter than that of **PBI-1**$_{Agg}$ obtained without sonication (Figure 5b,c, Supporting Information Figures S15 and S16). In accordance with the AFM images cryogenic scanning electron microscopy (cryo-SEM) confirmed the transformation from long fibrous aggregates into small seeds upon ultrasonication (Supporting Information Figures S17). In addition, while too strong scattering precluded the analysis of samples containing elongated nanofibers, dynamic light scattering (DLS) experiments for **PBI-1**$_{Seed}$ in solution afforded hydrodynamic radii from 10 to 780 nm size whose distribution is strongly dependent on the scattering angle, suggesting the presence of nonspherical aggregates (Supporting Information Figure S18). Accordingly, cryo-SEM and DLS studies support the conclusions from AFM with regard to the ultrasonic effect on the length of the supramolecular polymer, while the stacking mode between the PBI building blocks remains unchanged.

The seeded polymerization of **PBI-1** was evaluated at a temperature of 303 K by monitoring the time-dependent absorption changes at 530 nm for the transformation from the monomeric state to the aggregate state. Both **PBI-1**$_{Mono}$ and **PBI-1**$_{Seed}$ solutions were prepared as described above. Under the chosen conditions ($2 \times 10^{-5}$ M, 303 K) the monomeric species in toluene is a kinetically trapped state, and a spontaneous polymerization is prevented during the lag time of 1 h (Figure 4d, 303 K). In contrast, when a small amount of **PBI-1**$_{Seed}$ was added to a freshly prepared monomer solution (ratio between **PBI-1** molecules that exist in monomeric form to **PBI-1** molecules that are incorporated in seeds [**PBI-1**$_{Mono}$]$_0$/[**PBI-1**$_{Seed}$]$_0$ = $6.2 \times 10^2$), polymerization was initiated without a lag time (Figure 6a, curve I). It is noteworthy that no such polymerization kinetics was observed by addition of a MCH/toluene solvent mixture only (Figure 6a, curve II), which suggests the supramolecular polymer was propagated from the **PBI-1**$_{Seed}$. AFM and cryo-SEM images taken from the reaction vessel clearly confirmed the growth of the supramolecular polymers after the seeded polymerization initiated by the addition of **PBI-1**$_{Seed}$ (Figure 6b, Supporting Information Figures S19 and S17). These results indicate that the monomers attach to the termini of the nanofibers similar to conventional living polymerization process.[25] Interestingly, the polymerization rate was dramatically decreased when the long **PBI-1**$_{Agg}$ fibers were added instead of **PBI-1**$_{Seed}$ (Figure 6a, curve III), corroborating the notion that the **PBI-1**$_{Agg}$ sample has less concentration of "active" termini because the fiber length is longer than that of **PBI-1**$_{Seed}$ (Figure 5b,c).

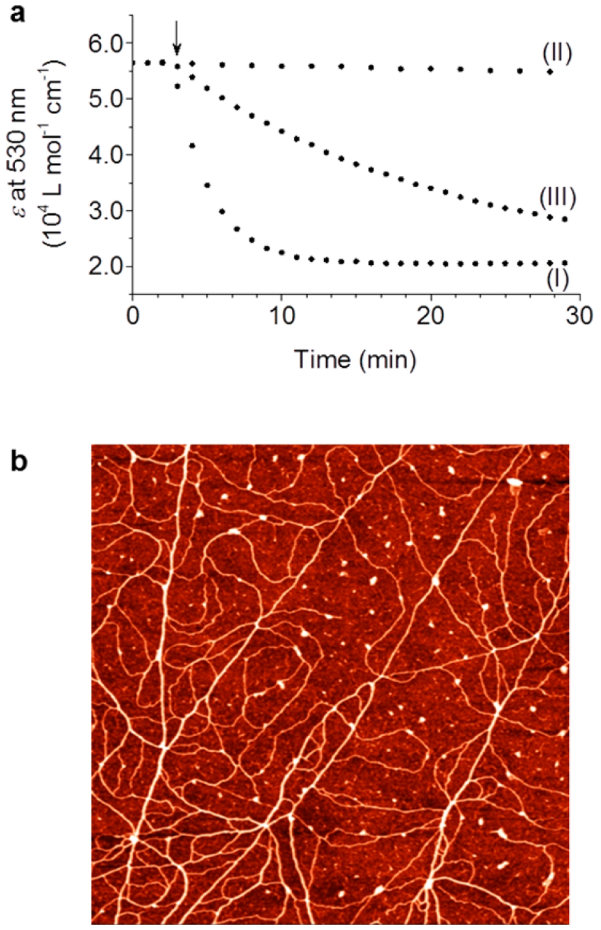


**Figure 6.** (a) Time course of the change in absorbance at 530 nm before and after addition of 10 $\mu$L MCH/toluene solution (2:1, v/v) of either **PBI-1**$_{Seed}$ (I), no **PBI-1** (II), or **PBI-1**$_{Agg}$ (III) to 3 mL of **PBI-1**$_{Mono}$ in toluene at a certain time (indicated by an arrow). Conditions: [**PBI-1**$_{Mono}$] = $2 \times 10^{-5}$ M, [**PBI-1**$_{Seed}$]$_0$ = [**PBI-1**$_{Agg}$]$_0$ = $1 \times 10^{-5}$ M, [**PBI-1**$_{Mono}$]$_0$/[**PBI-1**$_{Seed}$]$_0$ = [**PBI-1**$_{Mono}$]$_0$/[**PBI-1**$_{Agg}$]$_0$ = $6.2 \times 10^2$, 303 K. [**PBI-1**$_{Seed}$]$_0$ and [**PBI-1**$_{Agg}$]$_0$ refer to the concentration of PBI monomers embedded in seeds and aggregates, respectively. (b) AFM height image ($10 \times 10$ $\mu$m, the $z$ scale is 7 nm) of aggregate samples obtained after the seeded polymerization of **PBI-1** initiated by the addition of **PBI-1**$_{Seed}$ (plot I in (a)).

The seeded polymerization kinetics can be analyzed by the model proposed by Zhao and Moore[5] according to eq 1:

$$-\frac{d[M]}{dt} = k[M]c^* - k_-c^* = ([M] - [M]_\infty)kc^* \quad (1)$$

where $k$ and $k_-$ are the rate constants for the formation and dissociation of supramolecular polymers longer than nuclei, [M] is the monomer concentration, $[M]_\infty$ (= $k_-/k$) corresponds to the concentration of the monomer coexisting with supramolecular polymers at polymerization equilibrium, and $c^*$ is the concentration of added **PBI-1**$_{Seed}$ termini that associate with monomers. Integration of eq 1 gives eq 2:

$$[M] - [M]_\infty = ([M]_0 - [M]_\infty) \exp(-kc^*t) \quad (2)$$

where $[M]_0$ is the initial monomer concentration. The experimental data (curve I in Figure 6a) were fitted indeed very well by eq 2, giving the values of $[M]_\infty = 7.5 \times 10^{-6}$ M


DOI: 10.1021/ja511952c
J. Am. Chem. Soc. 2015, 137, 3300−3307

and $kc^* = 6.7 \times 10^{-3}$ $s^{-1}$ (Figure 7, black dots). Furthermore, the polymerization reaction was performed in several batches with different amount of added **PBI-1**$_{Seed}$ (Figure 7, colored dots).

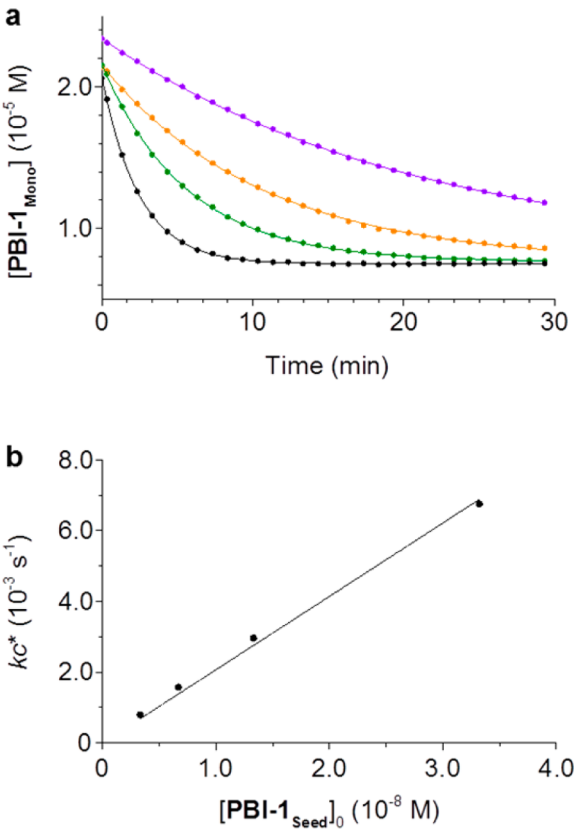


**Figure 7.** (a) Plots of the decrease in the monomer concentration ([**PBI-1**$_{Mono}$]) as a function of time after the supramolecular polymerization of **PBI-1** was initiated by the addition of **PBI-1**$_{Seed}$ under the conditions of $[\textbf{PBI-1}_{Mono}]_0/[\textbf{PBI-1}_{Seed}]_0 = 7.0 \times 10^3$ (purple), $3.2 \times 10^3$ (orange), $1.6 \times 10^3$ (green), $6.2 \times 10^2$ (black) at a temperature of 303 K. The solid lines were obtained by fitting the data to the seeded polymerization model (eq 2). (b) Plot of the $kc^*$ values as a function of $[\textbf{PBI-1}_{Seed}]_0$, showing a linear relationship (correlation coefficient 0.997).

**Table 1. Parameters $[M]_\infty$, $kc^*$ Obtained by Fitting of the Time-Dependent Data at 303 K to the Seeded Polymerization Model (eq 2)**

| $[\textbf{PBI-1}_{Seed}]_0$ ($M^{-1}$) | $[\textbf{PBI-1}_{Mono}]_0/[\textbf{PBI-1}_{Seed}]_0$ | $[M]_\infty$ ($10^{-6}$ M) | $kc^*$ ($10^{-3}$ $s^{-1}$) |
|---|---|---|---|
| $3.3 \times 10^{-8}$ | $6.2 \times 10^2$ | 7.5 | 6.8 |
| $1.3 \times 10^{-8}$ | $1.6 \times 10^3$ | 7.6 | 3.0 |
| $6.7 \times 10^{-9}$ | $3.2 \times 10^3$ | 7.6 | 1.6 |
| $3.3 \times 10^{-9}$ | $7.0 \times 10^3$ | 8.0 | 0.8 |

Fitting each polymerization to the model gave an almost identical value for $[M]_\infty$ (Table 1), suggesting that the addition of seeds has no meaningful influence on the monomer concentration at the polymerization equilibrium.[5,26] Importantly, a linear relationship between the $kc^*$ value and the amount of added **PBI-1**$_{Seed}$ is observed (Figure 7b); the slope of $2.1 \times 10^5$ $M^{-1}$ $s^{-1}$ is a rate constant that depends on the catalytic activity of the seed termini which can, however, not be determined due to the difficulty encountered in the determination of $c^*$. Nevertheless, the linear relationship indicates that the preformed **PBI-1**$_{Seed}$ has equal activity to associate with monomers in the supramolecular polymerization process. Accordingly, the time course of the supramolecular polymerization is well controllable by changing the amount of added **PBI-1**$_{Seed}$. Such a kinetic control over the self-assembling process based on the "seeding" approach is of significance for growth of supramolecular polymers with a narrow length distribution.[5,9]

## CONCLUSIONS

Looking at the literature of research on self-assembled $\pi$-conjugated materials and supramolecular polymers, we see a large gap between available molecular structures—thousands of molecules were shown to enable supramolecular polymerization by hydrogen-bonding and/or $\pi-\pi$-stacking interactions—and existing insights with regard to the exact supramolecular organization, average size, polydispersity, ordering, and homogeneity, etc. The latter features obviously require mechanistic insight into the supramolecular polymerization mechanism. Such insights were derived in the present study using both thermodynamic and kinetic analyses on a perylene bisimide organogelator molecule which can be assumed to be a good model also for hundreds of other molecules of similar design (hydrogen-bonding combined with $\pi-\pi$ stacking). Our spectroscopic and microscopic studies provided novel insights into the polymerization process of this archetype organogelator molecule: (1) the polymerization proceeds through nucleation followed by elongation processes; (2) the monomeric state can be kinetically trapped in a conformationally restricted state (here an intramolecularly hydrogen-bonded state); therefore, the spontaneous nucleation can be retarded; and (3) the supramolecular polymerization can be initiated by aggregate seeds that can be separately prepared (here, through sonication). Our results for the supramolecular polymerization of a perylene bisimide organogelator confirm a previous study that demonstrated for the first time the living character of seed-driven supramolecular polymerizations for a porphyrin molecule.[9] While the former example appeared to be a rather special case owing to the trapping of dye molecules within a second thermodynamically unstable off-pathway aggregate species, our current results demonstrate the more general possibility of inhibited nucleation of monomers by molecular design. Therefore, we assume that based on the protocol of thermodynamic and kinetic analysis provided in this paper, appropriate conditions for seeded living supramolecular polymerizations can also be identified for many other molecules, in particular for those derived from the huge class of organogelators. In addition we anticipate that our efforts to assess the generality of "seeding" polymerization approach will enable assembly of various $\pi$-conjugated molecules into unprecedented supramolecular polymer architectures including block copolymers.[7,8] Furthermore, the functionalization of seeds themselves would have a great potential for controlling not only the nanostructures but also the optical and electrical properties of organic materials.

## ASSOCIATED CONTENT

### Supporting Information

Analyses of self-assembling behavior of **PBI-1**, by UV–vis and IR spectroscopy, and AFM, cryo-SEM, and DLS studies on **PBI-1** aggregate samples. This material is available free of charge via the Internet at http://pubs.acs.org.



DOI: 10.1021/ja511952c
J. Am. Chem. Soc. 2015, 137, 3300–3307

## AUTHOR INFORMATION


### Corresponding Author

*wuerthner@chemie.uni-wuerzburg.de


### Notes

The authors declare no competing financial interest.

## ACKNOWLEDGMENTS

S.O. thanks the JSPS Postdoctoral Fellowship for Research Abroad for financial support.

## REFERENCES


(1) (a) Babu, S. S.; Praveen, V. K.; Ajayaghosh, A. *Chem. Rev.* **2014**, *114*, 1973−2129. (b) Aida, T.; Meijer, E. W.; Stupp, S. I. *Science* **2012**, *335*, 813−817. (c) de Greef, T. F. A.; Meijer, E. W. *Aust. J. Chem.* **2010**, *63*, 596−598.

(2) (a) Henson, Z. B.; Müllen, K.; Bazan, G. C. *Nat. Chem.* **2012**, *4*, 699−704. (b) Würthner, F.; Meerholz, K. *Chem.—Eur. J.* **2010**, *16*, 9366−9373.

(3) (a) Tidhar, Y.; Weissman, H.; Wolf, S. G.; Gulino, A.; Rybtchinski, B. *Chem.—Eur. J.* **2011**, *17*, 6068−6075. (b) Rybtchinski, B. *ACS Nano* **2011**, *5*, 6791−6818. (c) Rosen, B. M.; Peterca, M.; Morimitsu, K.; Dulcey, A. E.; Leowanawat, P.; Resmerita, A.-M.; Imam, M. R.; Percec, V. *J. Am. Chem. Soc.* **2011**, *133*, 5135−5151. (d) Roche, C.; Sun, H.-J.; Prendergast, M. E.; Leowanawat, P.; Partridge, B. E.; Heiney, P. A.; Araoka, F.; Graf, R.; Spiess, H. W.; Zeng, X.; Ungar, G.; Percec, V. *J. Am. Chem. Soc.* **2014**, *136*, 7169−7185. (e) Korevaar, P. A.; Newcomb, C. J.; Meijer, E. W.; Stupp, S. I. *J. Am. Chem. Soc.* **2014**, *136*, 8540−8543.

(4) (a) Kasai, M.; Asakura, S.; Oosawa, F. *Biochim. Biophys. Acta* **1962**, *57*, 22. (b) Asakura, S.; Eguchi, G.; Iino, T. *J. Mol. Biol.* **1964**, *10*, 42.

(5) Zhao, D.; Moore, J. S. *Org. Biomol. Chem.* **2003**, *1*, 3471−3491.

(6) (a) Wang, X.; Guerin, G.; Wang, H.; Wang, Y.; Manners, I.; Winnik, M. A. *Science* **2007**, *317*, 644−647. (b) Gilroy, J. B.; Gädt, T.; Whittell, G. R.; Chabanne, L.; Mitchels, J. M.; Richardson, R. M.; Winnik, M. A.; Manners, I. *Nat. Chem.* **2010**, *2*, 566−570. (c) Patra, S. K.; Ahmed, R.; Whittell, G. R.; Lunn, D. J.; Dunphy, E. L.; Winnik, M. A.; Manners, I. *J. Am. Chem. Soc.* **2011**, *133*, 8842−8845.

(7) (a) Qiu, H.; Russo, G.; Rupar, P. A.; Chabanne, L.; Winnik, M. A.; Manners, I. *Angew. Chem., Int. Ed.* **2012**, *51*, 11882−11885. (b) Rupar, P. A.; Chabanne, L.; Winnik, M. A.; Manners, I. *Science* **2012**, *337*, 559−562.

(8) Zhang, W.; Jin, W.; Fukushima, T.; Saeki, A.; Seki, S.; Aida, T. *Science* **2011**, *334*, 340−343.

(9) Ogi, S.; Sugiyasu, K.; Manna, S.; Samitsu, S.; Takeuchi, M. *Nat. Chem.* **2014**, *6*, 188−195.

(10) Würthner, F. *Nat. Chem.* **2014**, *6*, 171−173.

(11) Huang, C.; Barlow, S.; Marder, S. R. *J. Org. Chem.* **2011**, *76*, 2386−2407.

(12) Zhan, X.; Facchetti, A.; Barlow, S.; Marks, T. J.; Ratner, M. A.; Wasielewski, M. R.; Marder, S. R. *Adv. Mater.* **2011**, *23*, 268−284.

(13) (a) Würthner, F. *Chem. Commun.* **2004**, 1564−1579. (b) Seki, T.; Lin, X.; Yagai, S. *Asian J. Org. Chem.* **2013**, *2*, 708−724.

(14) (a) Li, X.-Q.; Stepanenko, V.; Chen, Z.; Prins, P.; Siebbeles, L. D. A.; Würthner, F. *Chem. Commun.* **2006**, 3871−3873. (b) Ghosh, S.; Li, X.-Q.; Stepanenko, V.; Würthner, F. *Chem.—Eur. J.* **2008**, *14*, 11343−11357. (c) Stepanenko, V.; Li, X.-Q.; Gershberg, J.; Würthner, F. *Chem.—Eur. J.* **2013**, *19*, 4176−4183.

(15) (a) Percec, V.; Ungar, G.; Peterca, M. *Science* **2006**, *313*, 55−56. (b) Jonkheijm, P.; van der Schoot, P.; Schenning, A. P. H. J.; Meijer, E. W. *Science* **2006**, *313*, 80−83. (c) De Greef, T. F. A.; Smulders, M. M. J.; Wolffs, M.; Schenning, A. P. H. J.; Sijbesma, R. P.; Meijer, E. W. *Chem. Rev.* **2009**, *109*, 5687−5754.

(16) Smulders, M. M. J.; Nieuwenhuizen, M. M. L.; de Greef, T. F. A.; van der Schoot, P.; Schenning, A. P. H. J.; Meijer, E. W. *Chem.—Eur. J.* **2010**, *16*, 362−367.

(17) Smulders, M. M. J.; Schenning, A. P. H. J.; Meijer, E. W. *J. Am. Chem. Soc.* **2008**, *130*, 606−611.

(18) Goldstein, R. F.; Stryer, L. *Biophys. J.* **1986**, *50*, 583−599.

(19) Chen, Z.; Fimmel, B.; Würthner, F. *Org. Biomol. Chem.* **2012**, *10*, 5845−5855.

(20) (a) Cui, H. G.; Chen, Z. Y.; Zhong, S.; Wooley, K. L.; Pochan, D. J. *Science* **2007**, *317*, 647−650. (b) Korevaar, P. A.; George, S. J.; Markvoort, A. J.; Smulders, M. M. J.; Hilbers, P. A. J.; Schenning, A. P. H. J.; De Greef, T. F. A.; Meijer, E. W. *Nature* **2012**, *481*, 492−496.

(21) Gellman, S. H.; Dado, G. P.; Liang, G.-B.; Adams, B. R. *J. Am. Chem. Soc.* **1991**, *113*, 1164−1173.

(22) Nowick, J. S.; Abdi, M.; Bellamo, A.; Love, J. A.; Martinez, E. J.; Noronha, G.; Smith, E. M.; Ziller, J. W. *J. Am. Chem. Soc.* **1995**, *117*, 89−99.

(23) (a) Bachmann, P. A.; Luisi, P. L.; Lang, J. *Nature* **1992**, *357*, 57−59. (b) Lohr, A.; Würthner, F. *Angew. Chem., Int. Ed.* **2008**, *47*, 1232−1236. (c) Carnall, J. M. A.; Waudby, C. A.; Belenguer, A. M.; Stuart, M. C. A.; Peyralans, J. J.-P.; Otto, S. *Science* **2010**, *327*, 1502−1506.

(24) Baldwin, R. L. *Folding Des.* **1996**, *1*, R1−R8.

(25) *Principles of Polymerization*, 4th ed.; Odian, G., Ed.; Wiley-VCH: Hoboken, NJ, 2004.

(26) (a) Nakaoka, Y.; Kasai, M. *J. Mol. Biol.* **1969**, *44*, 319−332. (b) Gerber, B. R.; Asakura, S.; Oosawa, F. *J. Mol. Biol.* **1973**, *74*, 467−487.




DOI: 10.1021/ja511952c
*J. Am. Chem. Soc.* 2015, 137, 3300−3307